Accepted Manuscript

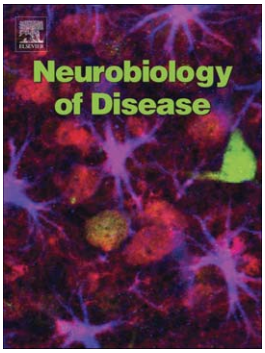

Recombinant adeno associated viral (AAV) vector type 9 delivery of Ex1-Q138-mutant huntingtin in the rat striatum as a short-time model for *in vivo* studies in drug discovery

Ilaria Ceccarelli, Pasquale Fiengo, Rosaria Remelli, Vincenzo Miragliotta, Lara Rossini, Irene Biotti, Alessandra Cappelli, Lara Petricca, Salvatore La Rosa, Andrea Caricasole, Giuseppe Pollio, Carla Scali

PII: S0969-9961(15)30097-8
DOI: doi: 10.1016/j.nbd.2015.11.019
Reference: YNBDI 3644

To appear in: *Neurobiology of Disease*

Received date: 24 June 2015
Revised date: 30 September 2015
Accepted date: 23 November 2015

Please cite this article as: Ceccarelli, Ilaria, Fiengo, Pasquale, Remelli, Rosaria, Miragliotta, Vincenzo, Rossini, Lara, Biotti, Irene, Cappelli, Alessandra, Petricca, Lara, La Rosa, Salvatore, Caricasole, Andrea, Pollio, Giuseppe, Scali, Carla, Recombinant adeno associated viral (AAV) vector type 9 delivery of Ex1-Q138-mutant huntingtin in the rat striatum as a short-time model for *in vivo* studies in drug discovery, *Neurobiology of Disease* (2015), doi: 10.1016/j.nbd.2015.11.019

Recombinant Adeno Associated Viral (AAV) vector type 9 delivery of Ex1-Q138-mutant huntingtin in the rat striatum as a short-time model for *in vivo* studies in drug discovery.

Ilaria Ceccarelli[1], Pasquale Fiengo[2], Rosaria Remelli, Vincenzo Miragliotta[3], Lara Rossini[4], Irene Biotti, Alessandra Cappelli, Lara Petricca[5], Salvatore La Rosa[6], Andrea Caricasole[5], Giuseppe Pollio and Carla Scali.

Siena Biotech S.p.A, Strada del Petriccio e Belriguardo, 35 53100 Siena (Italy)

Corresponding author:

Carla Scali PhD

Siena Biotech S.p.A

Strada del Petriccio e Belriguardo, 35

53100 Siena (Italy)

Tel +39 0577 381499

e-mail: carla.scali@outlook.com

Present Address

[1]*Dept. of Medicine, Surgery and Neuroscience, University of Siena. via Aldo Moro, 2- 53100 Siena (Italy)*

[2]*GlaxoSmithKline, via Fiorentina 1, 53100 Siena (Italy)*

[3]*Dept. of Veterinary Sciences, University of Pisa, Viale delle Piagge 2, 56124 Pisa (Italy)*

[4]*TesPharma S.r.l., Via P. Togliatti 20, 06073 Taverne di Corciano Perugia (Italy)*

[5] *IRBM, Via Pontina km 30,600, 00040 Pomezia Roma (Italy)*

[6]*Children's Tumor Foundation, 120 Wall Street, 16th floor, 10005New York NY (USA)*

Abstract

Huntington's disease (HD) is an inherited neurodegenerative disorder characterized by dyskinesia, cognitive impairment and emotional disturbances, presenting progressive neurodegeneration in the striatum and intracellular mutant Huntingtin (mHTT) aggregates in various areas of the brain. Recombinant Adeno Associated Viral (rAAV) vectors have been successfully used to transfer foreign genes to the brain of adult animals. In the present study we report a novel *in vivo* rat HD model obtained by stereotaxic injection of rAAV serotype2/9 containing Exon1-Q138 mHTT (Q138) and Exon1-Q17 wild type HTT (Q17; control), respectively in the right and in the left striatum, and expressed as C-terminal GFP fusions to facilitate detection of infected cells and aggregate production. Immunohistochemical analysis of brain slices from animals sacrificed twenty-one days after viral infection showed that Q138 injection resulted in robust formation of GFP-positive aggregates in the striatum, increased GFAP and microglial activation and neurodegeneration, with little evidence of any of these events in contralateral tissue infected with wild type (Q17) expressing construct. Differences in the relative metabolite concentrations (N-Acetyl Aspartate/Creatine and Myo-Inositol/Creatine) were observed by H1 MR Spectroscopy. By quantitative RT-PCR we also demonstrated that mHTT induced changes in the expression of genes previously shown to be altered in other rodent HD models. Importantly, administration of reference compounds previously shown to ameliorate the aggregation and neurodegeneration phenotypes in preclinical HD models was demonstrated to revert the mutant HTT-dependent effects in our model. In conclusion, the AAV2/9-Q138/Q17 exon 1 HTT stereotaxic injection represents a useful first-line in vivo preclinical model for studying the biology of mutant HTT exon 1 in the striatum and to provide early evidence of efficacy of therapeutic approaches.

Keywords: Huntington's disease, viral vectors, neurodegeneration, neuroinflammation immunohistochemistry, animal model, in vivo spectroscopy, gene expression.

Abbreviations used:

HD, Huntington's Disease, mHTT, mutant Huntingtin, rAAV, Recombinant Adeno Associated Virus, LV lentivirus, tNAA, total N-Acetyl Aspartate, Myo-Ins, Myoinositol, GFP, green fluorescent protein, NeuN, Neuronal nuclei, DARPP-32, dopamine- and cyclic AMP-regulated phosphoprotein, ChAT, Choline Acetyl Transferase, GFAP, Glial fibrillary acidic protein, Iba-1, ionized calcium binding adaptor molecule 1, PBST, phosphate buffered saline-Triton-X100, BSA, bovine serum albumin, DAB, diaminobenzidine, ROI, Region Of Interest.

Introduction

Huntington's Disease (HD) is an inherited neurodegenerative disorder characterized by dyskinesia, cognitive impairment, emotional disturbances and metabolic disorders, predominantly associated with progressive neurodegeneration of medium-spiny neurons in the striatum and with the presence of intracellular Huntingtin (HTT) aggregates in various areas of the brain.

The mutation responsible for HD has been identified as a CAG expansion within the Exon 1 of HTT gene (IT15, located on chromosome 4p16.3), which is translated into a polyQ stretch at the protein level (The Huntington's Disease Research Collaborative Group, 1993; reviewed by Ross and Tabrizi, 2011, Ha et al., 2012; Bates et al., 2015). Individuals with 35 CAG repeats or fewer do not develop HD, while repeats of 40 and above are invariably associated with disease appearance (Myers et al., 1988).

Currently there is no effective treatment for preventing or delaying the disease, which typically sets in at around 35-45 years of age and progresses towards death within 10-20 years after the appearance of the first clinical symptoms. It is crucial from a drug discovery prospective to create animal models that, in addition to presenting symptoms typical of striatal neurodegeneration, also recapitulate the genetic and molecular mechanisms underlying the degenerative processes of the human pathology. To that end, the combination of knowledge of the genetic basis of the disease and the emergence of transgenic and gene transfer technologies has allowed the creation of animal models of HD (from the invertebrate C. Elegans to primates) that recapitulate the genetic defect found in humans and are able to reproduce phenotypes reminiscent of HD such as nuclear huntingtin inclusions, neurodegeneration, motor deficits and cognitive impairment (Menalled 2005, Ramaswamy et al., 2007, Fecke et al., 2009). In most cases, these models are based on mutant huntingtin bearing ca. 100 or more glutamines (e.g. R6/2, BACHD, YAC128 and Knock-In mice, with ca. 130, 97, 128 and 111 polyglutamine repeats respectively; Ferrante 2009; Menalled and Brunner., 2014). Polyglutamine expansions larger than observed in adult-onset HD and closer to those observed in the earlier onset, more aggressive juvenile HD are often required to create robust aggregation and pathology in rodent models. However, despite the availability of several models and intensive efforts on the part of drug developers to date no clinical data exists to support the translational value of preclinical models for HD patients. Mammalian models of HD are dominated by the use of rodents (especially mice) which historically represent the mammalian species of choice for the generation of genetic models. Several rodent lines have been generated expressing mutant huntingtin as transgenic (either as full length protein or as N-terminal fragments) or knock-in models, which in some cases have been extensively characterized at the molecular, histopathological as well as behavioural/cognitive level. The severity of the phenotypes produced as

well as their resemblance to human HD is typically stronger in models expressing N-terminal fragments, and in particular in those expressing the protein fragment encoded by exon 1 (Mangiarini et al, 1996; Gray et al, 2008; , Slow et al., 2003; etc.; reviewed in Lee et al. 2013). In spite of the usefulness of these models to investigate disease mechanisms, drug efficacy trials in most of these rodent models (including exon 1 models) require labour-, time- and cost-intensive studies, lasting several months to more than a year and typically requiring relatively large cohorts of animals. The availability of relatively more rapid, less resource intensive in vivo models, reproducing key aspects of the human pathology and bridging the gap between in vitro neuronal models and the more pathophysiologically relevant but low-throughput genetic models would greatly facilitate the evaluation of therapeutic approaches at an early stage of the drug discovery process. In vivo viral gene transfer models represent an opportunity to address this need. Recombinant Adeno Associated Viral (rAAV) vectors have been successfully used to transfer genes in a variety of tissues, including brain, in adult animals (Burger et al., 2004, Tenebaum et al., 2004, and McFarland et al., 2009; Huda et al. 2014). Moreover rAAV vectors have also been widely used in clinical trials for neurodegenerative diseases and have been shown to be more effective at transducing certain brain regions compared to lentiviral vectors (de Backer et al., 2010). The first rAAV-based HD model employed to express along CAG repeat fused to green fluorescent protein (GFP) in the rat striatum, described a rapid formation of fibrillar, cytoplasmic and ubiquinated nuclear polyglutamine aggregates as well as neurotoxicity (Senut et al 2000).

In the present study we used rAAV2/9, expressing Exon 1 HTT carrying 17 or 138 CAG repeats (wild type and mHTT, respectively) to implement and optimize a rat model of HD. As the envisaged model was of an acute nature, a long (Q138) polyglutamine repeat was selected in order to maximize chances of eliciting a robust pathology-relevant response and for polyQ length coherence with one of the transgenic mouse HD models most widely employed for drug screening, namely the R6/2 mouse (Mangiarini et al., 1996). AAV2/9-Exon1-GFP/Q138 (AAV9-Q138) was injected in the right striatum and AAV2/9-Exon1-GFP/Q17 (AAV9-Q17) in the left striatum as control and neurodegeneration and neuroinflammation markers were evaluated by immunohistochemical analysis. In order to test whether our model could recapitulate the hallmarks of the transcriptional imbalance found in HD patients and other models, we also performed qRT-PCR on AAV injected striata on selected genes known to be dysregulated in HD. Magnetic Resonance Imaging and ^{1}H MR Spectroscopy was carried out to evaluate the morphological and metabolic changes induced by mHTT expression. Finally, we validated this in vivo model as a tool for drug screening by demonstrating reduction of the phenotypic responses to mHTT by pharmacological treatment with a tool compound known to be active in reducing aggregation and neurodegeneration in preclinical

HD models, namely the transglutaminase inhibitor Cystamine (Dedeoglu et al., 2002; Van Raamdsonk et al 2005).

Methods

Plasmids construction and rAAV particles preparation

The exon1 of human HTT gene (GenBank: L27350.1) was amplified by proofreading PCR using specific primers carrying an EcoRI site at the 5'-end and a BamHI site at the 3'-end, using as template a full-length HTT cDNA including a mixed CAG/CCA repeats, coding for a poly Q tract (Wittenbach et al., 2001; Smith et al., 2014).

The amplicons, named exon1-HTT-Q17 and exon1-HTT-Q138, respectively, were cloned in frame with AcGFP into the pAcGFP-N1 vector (Clontech, NJ USA) fused at C-terminal end of exon 1. The obtained AcGFP-exon1-HTT-Q17/Q138 fragments were then inserted into pcDNA3.1zeo+ vector (Invitrogen, UK). The final expression vectors were obtained subcloning the cDNA sequence for AcGFP-exon1-HTT-Q17/Q138 from pcDNA3.1zeo+ into pAAV-CAG-cis plasmid (Vector Biolabs, PA). The oligonucleotides used for PCR amplification are listed as follow:

Primer EcoRI-HTT-For: 5'-AAGAATTCACCATGGCGACCCTGGAA-3'

Primer BamHI-HTT-exon1-Q17/Q138 –Rev: 5'-AAGGATCCCCTCGGTGCAGCGGCTCC-3'.

AAV particles were prepared by Vector Biolabs (Philadelphia, PA USA).

Animals

Forty four female Wistar rats (175-200g) (Harlan Italy) were used in this study. The animals were housed in a controlled temperature (20-24°C) and humidity (40-70%) room maintained on a 12 hr dark/light cycle. Animals were placed in individually ventilated solid floor plastic cages (IVC Sealsafe® Plus GR900, Tecniplast, Italy), 3 animals/cage. Food and water were available *ad libitum*. Animal experiments were carried out in conformity to the guidelines of the European Community's Council for Animal Experiments (86/609/EEC and 2010/63/EU) and the Principle of Laboratory Animal Care. All efforts were made to minimize the number of animals used and their suffering. In the present study 10 animals were used in a pilot study to evaluate the development of infection and formation of aggregates; they were sacrificed 48h, 7d, 14d and 21d after surgery (N=2/3 per groups). The remaining 34 rats were sacrificed at 21d after surgery according to the scheme reported in supplementary information (Fig. 1S) and used for morphological determination and reference compound treatment (N=26), transcriptional analysis (N=3) and Magnetic Resonance Imaging and H1 MR Spectroscopy determinations (N=5).

Drugs

Cystamine dihydrochloride

Cystamine dihydrochloride (Sigma Chemical Co., MO, USA 333 mg/mL) was dissolved in Dulbecco's PBS and used to fill osmotic minipumps (2ML4, Alzet, CA, USA) for the subcutaneous deliver of 100 mg/Kg/day of the compound continuously for 21 days.

Stereotactic surgery

Animals were deeply anesthetized (2-3% isoflurane, 60% O_2, 40% N_2O) and gently fixed with ear bars and head holder in a stereotaxic apparatus (Stoelting, IL, USA). Four microliters of Adeno-Associated Virus (AAV9-Q138 or AAV9-Q17, $15.2x10^{10}$ Genome Copies, Vector Biolabs, USA) were injected in the right and in the left striatum, respectively (0.5 mm anterior; ±3.0 mm lateral to Bregma and 4.8 mm depth from dura, Paxinos and Watson 1998) by a Hamilton syringe (Hamilton, HV, USA) equipped with a 30 gauge blunt-tip (Fig 1). In animals treated with cystamine dihydroclorate, during viral injection, osmotic minipumps (2ML4, Alzet, CA, USA) were subcutaneously implanted in the upper part of the dorsum of the animal to continuously deliver the drug. After surgical suturing, rats were removed and individually caged until complete wound healing.

Tissue preparation

Twenty-one days after surgery animals were deeply anaesthetized (Tanax®, Intervet Italy) to be intracardially perfused with 4% paraformaldheyde, postfixed for 24 hours and cryoprotected with 18% sucrose. Slices (30 µm thickness) were cryo-sectioned (Leica Microsystem CM1950, Germany) and processed for immunohistochemistry or immunofluorescence.

Immunohistochemistry and immunofluorescence procedure

Slices were processed as free-floating sections. Briefly, the primary antibody was added at the appropriate dilution (in Blocking buffer: PBS with 0.5% BSA and 0.05 % Triton-X for tissue permeabilization and left overnight under gentle agitation at room temperature. For immunohistochemical detection, the slices were incubated with the appropriate biotinylated secondary antibody (Vector Laboratories, CA, USA) in Blocking buffer for 90 min at room temperature under mild agitation, and the bound antibody was visualized by using Vectastain ABC Kit and DAB (Vector Laboratories, CA, USA). The sections were mounted, counterstained with Ematossilin (Carlo Erba Reagents, Italy), dehydrated and coverslipped with mounting medium (Leica Biosystem, Germany). For immunofluorescence detection, the slices were incubated with the appropriate AlexaFluor-conjugated secondary antibody (Invitrogen) in Blocking buffer for 90 min at room temperature under mild agitation and mounted on a slide with mounting medium (Vectashield with DAPI, Vector Laboratories, CA, USA). The images were acquired by confocal

microscopy (Zeiss LSM 510 META, Germany) or fluorescence microscopy (Nikon Eclipse 90i Japan).

The primary antibodies used are: anti-HTT, clone EM48 (for aggregates, Millipore 1:1,000, Merk Millipore Germany), NeuN (marker of neuronal nuclei, mouse monoclonal antibody, Millipore, 1:500, Merk Millipore Germany), ChAT (choline acetyl transferase, marker of cholinergic neurons, goat antiserum, Millipore, 1:200, Merk Millipore Germany), DARPP-32 (dopamine- and cyclic AMP-regulated phosphoprotein, marker of medium spiny neurons, rabbit polyclonal antibody Millipore, 1:500, Merk Millipore Germany), GFAP (glial fibrillary acidic protein, marker of astrocytes, rabbit polyclonal antibody DAKO, 1: 1000, Agilent Technologies CA, USA), Iba-1 (ionized calcium binding adaptor molecule 1, marker of microglia, rabbit antibody, Wako, 1:500; Wako Germany).

Immunohistochemical marker quantification

All immunohistochemical markers were quantified on the entire striatal area by the Aperio digital pathology platform (Aperio Scanscope, Leica Biosystem, Germany); briefly, 4-6 slides per animal were digitalized by using the scanner then the right and left striata were manually identified for each slide creating a Region Of Interest (ROI) where specific macros of analysis were applied to quantify the signal. Each right striatum (AAV9-Q138) was compared with its contralateral (left) one (AAV9-Q17). Data from each slide were averaged on a per animal basis and the resulting values were used for statistical analysis.

NeuN was quantified as number of NeuN positive nuclei per area. ChAT was quantified as number of cells per area. DARPP-32, GFAP and Iba-1, were evaluated as positive pixel counts per area in the ROI.

In the right striatum (Q138), GFP signal was used to quantify the number and dimensions of GFP positive aggregates in the right striatum. In particular, three slices centered in the injection region spaced at 500µm, were acquired by fluorescence microscopy (Nikon Eclipse 90i, Japan) and subsequently quantified with Matlab (The Mathworks, Natick, USA) using the Otsu's method (Otsu et al., 1979) with minor modifications (La Rosa et al., 2013).

Transcriptional analysis of AAV9-Ex1-AcGFP-Q138 and AAV9-Ex1-AcGFP-Q17-injected striatum

For the analysis of mHTT-mediated transcriptional dysregulation, a small group of animals was sacrificed by decapitation, under deep anesthesia, to collect the right (AAV9-Q138) and left (AAV9-Q17) striatum. Samples were homogenized in RLT buffer (Qiagen, The Netherlands) and RNA was extracted with the kit ALL Prep DNA/RNA (Qiagen) according to manufacturer's instructions. One µg of mRNA isolated from the right and left striatum was retrotranscribed using the Quanti-Tect

Reverse Transcription-Kit (Qiagen, The Netherlands) according to the manufacturer's instructions. For every RNA sample two independent reverse transcriptase reactions were performed. Quantitative real-time PCR (RT-qPCR) was performed in triplicate for the analyzed genes using the C1000™ Thermal Cycler (Biorad, CA,USA). All reactions were performed in a total volume of 20 µl containing 10 ng cDNA, 10 µl iQ™ SYBR Green Supermix (Biorad, CA, USA) and 0.3 mM forward and reverse primers. The amounts of target gene mRNA were normalized to β-actin levels. The genes analyzed were 7DHCR, pENK, ADORA2A, DRD1 and DRD2 (Kuhn et al., 2007) and the PCR primers utilized are listed in Fig.4.

Magnetic Resonance Imaging and H1 MR Spectroscopy

Preclinical 1H-MRS experiments were performed with an MRI system (Bruker Pharmascan® 70/16, Germany) operating at 7 tesla (300Mhz for 1H). Circular polarized resonator optimized for rat brain was used for RF transmission while a dedicated quadrature 1H surface coil was positioned on the top of the rat brain. Localization of the volumetric region (voxel) in the striatum for the measurement of metabolite concentration was performed by a rapid magnetic resonance imaging survey of the brain where axial, coronal and sagittal images were recorded using fast spin-echo method. In the coronal plane (used for MRS exam), 18–21 images were recorded with a repetition time (TR) of 3000ms, an echo time (TE) of 33ms and total bandwidth of 50KHz. In all experiments, the image thickness was 1mm with an interslice distance of 1mm and acquisition time of about 8m:44sec. FAST-MAP method, combined with additional linear shimming steps, was applied on 3x3x3 mm voxel to shim the homogeneity of the magnetic field and optimize water suppression. The resulting waterline width was about 10Hz. Vapor water suppression scheme was applied prior of a Point REsolved Spectroscopy Sequence (PRESS) with TR was 3000msec, echo time TE 20msec, 256 averages and spectral width of 4Khz (2048 points) on 15.625uL (2.5x2.5x2.5 mm) voxels localized in left and right striatum according to AAV9-Q17 and AAV9-Q138 injection's sites. MRS spectra were fit using TARQUIN (Wilson et al. 2011) and metabolite concentrations were normalized in respect to control signal.

Statistic analysis

MRS derived metabolite concentrations as well as neurodegeneration, neuroinflammation and gene expression data from AAV9-Q138 versus AAV9-Q17 injected striata, were evaluated by paired Student's *t*-test with a significance level of $\alpha = 0.05$. Efficacy of reference compounds on neurodegenerative and neuroinflammation markers was evaluated on data normalized in respect to the contralateral area and then averaged on a per subject basis (Q138/Q17 ratio). Univariate statistical analyses of each marker were carried out applying non parametric one-way ANOVA

model (Kruskal Wallis) on treatment level as fixed effect with a significance level of $\alpha = 0.05$. Post Hoc pair-wise comparisons were performed using Dunnett multiple comparisons to evaluate treatment efficacy versus vehicle control group.

All statistical analyses were performed using GraphPad Prism 5.03 (GraphPad Software Inc, CA, USA) and Matlab (The Mathworks, Natick, USA).

Results

Generation of an AAV-based HD expression system for in vivo modeling

In order to develop an acute rat model of HD neurodegeneration useful as a first-line *in vivo* compound testing tool, we designed recombinant adeno-associated viral constructs for the delivery of the exon 1 of mutant huntingtin into the striatum. The AAV9 serotype was chosen for its ability to infect neuronal cells (Aschauer et al, 2013; Huda et al. 2014), as also confirmed through in house experiments with several AAV serotypes (data not shown). The exon 1 of mutant HTT with a polyQ expansion of >100 was chosen for its capacity to induce robust aggregation and neurotoxicity, and for its coherence with one of the transgenic mouse models of HD most widely employed for drug screening the R6/2 model (Mangiarini et al., 1996). Following generation of the plasmid constructs and production of the viral particles, these were tested for correct expression of the encoded mHTT-GFP fusion protein by infecting primary rat cortical neurons (Supplementary data Fig 2SA and B) and examining protein expression by Western blotting using an antibody specific for a huntingtin N-terminal epitope (EM48 antibody) (Fig. 2S C). Subsequently to positive outcome from in vitro study, AAV9-Q138, encoding mHTT-GFP, was injected in the right striatum of female rats, whereas the contralateral striatum was injected with the same number of genome copies of AAV9-Q17, carrying the an equivalent HTT-GFP with a wild-type expansion (Fig 1A). The principal objective was to establish a neuropathological model rather than a behavioural model, and therefore a monolateral AAV mHTT-GFP model, where the contralateral hemisphere is instead injected with AAV expressing wild type HTT-GFP as a control, was preferred for the advantages in morphological evaluation. The injection of AAV9-Q138 and AAV9-Q17 led to the infection of almost the entire striatum areas with marginal diffusion to corpus callosum (Fig 1B). During the observation period prior to sacrifice (3 weeks), daily clinical signs monitoring revealed no obvious abnormalities. Furthermore, a pilot evaluation of locomotor activities by rota-rod, reflected no impairments caused by monolateral AAV9-Q138 infection (data not shown) in line with findings from other laboratories although with different viral vector (de Almeida et al., 2002). It is pertinent to mention that Franich et al., (2008) reported behavioral deficit in AAV-injected animals.

The injection of AAV9-Q138 determined the appearance of GFP positive aggregates in the entire striatal area detectable mainly inside neuronal nuclei as fluorescent aggregates that superimpose on a more diffuse GFP fluorescence, as confirmed by confocal microscopy (Fig.1D). The aggregates appeared at a relatively early post-injection time (48 hours), increasing progressively as measured at day 7 and 15 and reaching the highest level of expression at day 21 (Fig. 3S, in supplementary materials), when aggregates positive to EM48 antibody were densely spread in the entire striatal area (Fig 1E); AAV9-Q17 injection resulted in a more diffused GFP signal, with some GFP-positive cells with neuronal-like morphology and the absence of aggregates, detected 21 days after virus injection (Fig. 1C). Co-staining with antibody NeuN for neuronal determination and GFAP for astroglial cells revealed that mHTT is predominantly expressed in neurons rather than astrocytes, although these latter are not resistant to AAV9 infection (Fig. 1 F-G). We also examined the microglia cells with an antibody against Iba-1, a protein upregulated in activated microglia (Ito et al, 1998). Many activated microglia cells that stained intensely with Iba-1 were detected around infected neurons in AAV9-Q138 striatum (Fig. 1 H) and some of them contained crumble mHTT aggregates presumably derived by macrophage function exerted by the activated cells although, as for astrocytes, a primary infection cannot be not excluded.

AAV9-Q138 HTT exon 1 induces neurodegeneration and neuroinflammation in the rat striatum

In order to quantify the decrease in NeuN-positive cells (neurons labelled with Neuronal Nuclei antibody) observed by immunofluorescence at 21 days post injection, we developed and optimized an automated segmentation-based analysis of the immunohistochemical signal. NeuN-positive cells have been used as histochemical markers of neurons and are widely employed for the quantification of neurodegeneration in various HD models, including an LV-based HD rat models (Regulier et al., 2003). The NeuN-positive cell density was significantly lower in the AAV9-Q138 injected side when compared to the AAV9-Q17-injected contralateral striatum (Fig 2 A-C and L, $t=7.684$, $d.f.=9$, $p<0.001$). DARPP-32, a regulator of dopamine receptor signaling is expressed in ca. 95% of medium size spiny neurons (MSNs) and is not expressed in other striatal cell types (Anderson and Reiner, 1991; Ouimet et al., 1998; Arlotta et al., 2008;). In order to quantify the degeneration of medium spiny neurons (MSNs), the most abundant neuronal type in the striatum and the most affected in HD, we also implemented a quantitative immunohistochemical analysis of DARPP-32, asDARPP-32 down regulation is an early marker of neuronal dysfunction in HD (Luthi-Carter et al., 2000, de Almeida et al., 2002, Bibb et al., 2000). Following AAV9-Q138 injection in the right striatum, DARPP-32 levels decreased compared to AAV9-Q17, especially in the area surrounding the injection site (Fig 3D-F and M). The quantification of DARPP-32 staining, expressed as positive

pixel counts within the striatal area, confirmed a statistically significant decrease of DARPP-32 signal in the AAV9-Q138 injected striatum.($t=5.608$, d.f.=8, $p<0.001$, Fig 2D-F and M). In addition, we also investigated the impact of AAV9-Q138 injection on striatal cholinergic (ChAT positive) neurons, a subpopulation of large size interneurons in the striatum. The number of ChAT positive neurons was lower in AAV9-Q138-injected striatum than in the AAV9-Q17-injected one ($t=7.356$, d.f.=9 $p<0.001$, Fig 2 G-I and N). Aperio Scanscope system used for the quantification of neurodegenerative markers allow the determination of the striatal area, revealing, no substantial shrinkage or modification of the striatal area at the selected period (3 weeks from AAV injection). Emerging evidence suggests a role of neuroinflammation in HD progression (Politis et al., 2015; Crotti and Glass, 2015). We therefore examined the neuroinflammatory response in the AAV9-Q138 injected striatum with the quantification of microglia and astrocytes. Although signs of glial activation were visible in the AAV9-Q17 contralateral striatum, several rounded, amoeboid microglia were exclusively detected in the AAV9-Q138 striatum (Fig 3A and C). Automated morphometrical quantification of microglial response in the right and left striatum showed a statistically significant increase in microglia activation in AAV9-Q138-injected striatum compared to the AAV9-Q17-injected ($t=9.058$, d.f.=8, $p<0.001$, Fig. 3 G).

As shown in Fig 3 D, E, F and G, GFAP-immunoreactivity was analyzed as an indicator of astrogliosis. As for microglia, Q138 injection induced massive activation of astrocytes. Automated morphometrical quantification of GFAP response in the right and left striatum (positive pixel count/area) showed a statistically significant increase in astrocytes activation in Q138-injected striatum with respect to Q17 ($t=2.83$, d.f.=8, $p<0.05$). Thus, the AAV9 HTT exon 1 model reproduces several histological phenotypes observed in HD and HD models, including EM48-positive protein aggregation, downregulation of striatal neuronal markers (including those for MSNs and cholinergic neurons), and glial activation (astrocytes and microglia) in a manner dependent on the presence of an expanded (mutant) polyglutamine repeat.

Although our focus was related to striatal area, during the pilot experiment aimed to reveal the amount of infection by mean GFP epifluorescence (Fig. 3S), we analyzed the amount of GFP signaling in the *globus pallidus* and *substantia nigra*, for evaluating the AAV vector axonal transport. Three weeks after viral injection a weak GFP labelling was observed (data not shown) and no further investigations were carried out. Notably, Franich et al. (2008) reported relevant degeneration also in these target areas detected at longer period (5 weeks after viral injection).

AAV9-Q138 HTT exon 1 induces transcriptional dysregulation in the rat striatum

We next asked if this model could reproduce some of the molecular changes associated with mutant HTT expression in other preclinical models, namely transcriptional dysregulation (e.g. see Kuhn et

al. 2007). Therefore, a quantitative RT-PCR was carried out on samples from AAV9-Q138 and AAV9-Q17-injected striata, and the expression of selected genes known to be dysregulated in HD models was examined: 7DHCR, pENK, ADORA2A, DRD1 and DRD2 (Kuhn et al., 2007; Valenza and Cattaneo, 2011). As for other studies (e.g. Kuhn et al., 2007), we focussed on striatal gene expression because the striatum is described as the HD brain region with the most dramatic neuropathology and the most robust mRNA changes. As shown in Fig 4, mHTT induced selective gene expression modulation, with steady-state mRNA levels of 7DHCR ($t=8.73$, $df=2$, $p<0.05$) A2a receptor ($t=5.37$, $df=2$, $p<0.05$), PENK ($t=26.67$, $df=2$, $p<0.01$), DRD1A ($t=10.12$, $df=2$, $p<0.01$) and DRD2 ($t=11.5$, $df=2$, $p<0.01$) receptors in Q138 injected mice are significantly decreased relatively to contralateral striata injected with the AAV9-Q17 encoding virus. We did not observe significant changes in striatal BDNF mRNA levels (data not shown), consistent with reports indicating the cortex as the principal corticostriatal site of BDNF expression (reviewed in Baydyuk and Xu, 2014). Therefore, the model can at least in part reproduce the transcriptional dysfunction induced by mutant HTT in other preclinical HD models.

AAV9-Q138 HTT exon 1 induces metabolic changes in the rat striatum.

1H Magnetic Resonance Spectroscopy (1H-MRS) allows in vivo measurement of prominent cerebral metabolites, including N-acetylaspartate (NAA) and *N*-acetylaspartylglutamate (NAAG) as neuronal integrity markers, Creatine (Cr) as a marker of the energetic status of the tissue and Myo-Inositol (Myo-Ins) as a glial cell marker (Zhu et al. 2006). Recent evidence demonstrates changes in the local concentrations of these metabolites in patients affected by Huntington's disease at pre-manifest and early stages (Sturrock et al. 2010). To evaluate effects induced by mutant and wild type HTT injection in striatal metabolite concentration, N-acetylaspartate (NAA), *N*-acetylaspartylglutamate (NAAG), Myo-Inositol (Myo-Ins) and Creatine (Cr) were detected by H1 Spectroscopy (Fig. 5 A and B) in AAV9-HTT injected animals. N-acetylaspartate (NAA) and *N*-acetylaspartylglutamate (NAAG) were analyzed as total NAA (tNAA). The tNAA/Cr and Ins/Cr ratio were calculated for each side (AAV9-Q17 and AAV9- Q138) and used for statistical analysis. Paired Student's *t*-test analysis showed that Myo-Ins/Cr (Fig. 5 C) was significant higher in the AAV9-Q138-injected side than in the AAV9-Q17-injected side ($t=-3.0066$ $d.f.=4$, $p<0.05$), while tNAA/Cr concentration (Fig. 5D) was lower in the AAV9-Q138 side with respect to the AAV9-Q17 injected side ($t=5.9771$, $d.f.=4$, $p<0.05$). Interestingly, therefore, the AAV9-Q138 striatal injection appears to induce some of the metabolic dysfunctions observed in patients during the early phases of the disease, further supporting the translational value of the model.

Reversal of AAV9-Q138 induced phenotypes by tool compound: validation of the model as *in vivo* tool for profiling candidate therapeutics

Having established that the AAV9-Q138-based model can reproduce a variety of phenotypes relevant to HD pathology, we sought to establish if these changes could be reverted by established, reference pharmacological treatments, an essential prerequisite for its utility as an *in vivo* drug screening tool. We selected Cystamine as a reference agent which previous studies have demonstrated to reduce the characteristic histopathological phenotypes in the R6/2 transgenic mouse model, expressing a mutant exon 1 HTT protein of comparable polyglutamine expansion to the AAV9-Q138 rat striatal model (Dedeoglu et al. 2002).

The effects of Cystamine (100 mg/kg/day sc via Alzet mini-pumps for 21 days) were analyzed on morphological parameters of neurodegeneration and neuroinflammation (NeuN, DARPP-32, ChAT, Iba-1) using the ratio between the AAV9-Q138- and AAV9-Q17-injected striatum.One-way ANOVA and Dunnett's post hoc test revealed that Cystamine significantly increased NeuN positive cells in respect to vehicle treated animals (Fig. 6B and C) (ANOVA $F(2,16)= 6.654$, $p<0.01$), while only a tendency toward amelioration was observed in other neurodegeneration (DARPP-32, Fig 6D) or neuroinflammation parameters (data not shown).

Discussion

The development of efficacious therapeutics for human neurodegenerative diseases is critically dependent on the availability of preclinical models faithfully reproducing the genetic, molecular and pathological events observed in patients. In particular, the translational value of *in vivo* models and readouts is one of the key factors associated with therapeutic success in the clinic. However, the most physio-pathologically relevant models are very often ill-suited to meet the necessity of rapid parallel probing of several potentially relevant therapeutic mechanisms with tool compounds in an *in vivo* setting, prior to full-scale prosecution of a target/mechanism with an integrated drug discovery and development program. This is a desired condition where knowledge of the molecular events associated with the pathology is relatively scarce, as in the case of neurodegenerative diseases such as HD. Therefore, a first-line *in vivo* model capable of handling multiple pharmacological interrogations with a battery of readouts reproducing those found in more complex, more pathophysiologically relevant (genetic) models and in human disease would increase the capacity and the turnover of therapeutics discovery, enabling the successive testing of the most promising candidate therapeutics in the longer, more complex trials in genetic models. We therefore sought to develop an acute *in vivo* model of HD capable of producing robust phenotypes comparable with those observed in one of the most widely employed HD mouse model, the R6/2 model. We demonstrated the relevance of this model in drug discovery processes by confirming the neuroprotective effect of a compound already shown to be effective in other HD models. To our

knowledge, these data consist in the first evidence of pharmacological modulation of the damages induced by mutant Htt in a viral-injected rodent model. Notably several elegant data have been produced using genetic modulation of protein expressions capable to counteract the insults produced by viral infections of mHtt (Franich et al., 2008, Popiel et al., 2012, Taylor et al 2013). Recombinant viral vectors-based models offer several advantages: they can be used in any mammalian species, the onset and temporal progression of the pathogenicity can be controlled by selecting the time and amount of viral vector, the transgene can be introduced in discrete areas of the CNS. As result, the use of viral vector constructs allows the generation of genetic rodent disease model more rapidly and more economically than is required for breeding and maintenance a colony of transgenic mice.

Recombinant AAV has emerged as one of vectors of choice for gene transfer to the CNS, because its transduction of dividing and non-dividing cells and strong neural tropism (Grieger and Samulski, 2012). The packaging capacity of 4.7 kilobases precludes AAV vector-mediated overexpression of full-length HTT, but N-terminal truncated HTT constructs have been successfully used previously to recapitulate some of the phenotypic characteristics of HD in experimental animals (de Almeida et al., 2002, DiFiglia et al., 2007) compared to the widely used HD transgenic mouse model Tg R6/2 (Mangiarini et al., 1996). It is pertinent to mention that several labs also developed robust HD models by producing LV infections in cells (Zala et al., 2005) and in rodent (rev. by Ruiz and Deglon 2012).

The AAV serotype used in the present study, AAV2/9, was selected among other phenotypes after testing in rat brain and evaluating the spreading of infection, the type of cell infected and the inflammatory response determined by the viral injection. From this preparatory study the rAAV2/9 serotype was chosen for its predominantly neuronal tropism, significant spreading and lower inflammatory response determined with respect to the other AAV phenotypes or other LV tested. The use of a double injection in the different brain hemispheres allows the direct comparison of the effects of WT HTT *versus* mutant HTT in the same animal, decreasing the inherent inter-subject variability during morphological analysis.

Our model is characterized by the appearance of intranuclear, cytoplasmic and neuritic aggregates very early following injection (48 hours), increasing progressively (7 and 15 days, data not shown) and reaching high levels by 21 days, when aggregates densely populate the entire striatal area. Intracellular aggregates observed in the present study resemble those previously described in a number of *in vitro* and *in vivo* studies. Indeed previous studies showed that both nuclear and neuritic aggregates are present in many HD transgenic mice (R6/2, N171-82Q and Hdh $^{80\ CAG}$). In R6/2 and Hdh $^{80\ CAG}$ knock-in mice the neuritic aggregates appear later than nuclear aggregates (Li et al., 1999, Schilling et al., 1999, Li et al., 2000). The disparity in aggregate load has been postulated to

be at least in part dependent on the levels of HTT expression, with low levels of mutant HTT favoring the formation of small and abundant aggregates in axons and dendrites, whereas the development of nuclear inclusions is associated by the presence of high levels of HTT (de Almeida et al., 2002).

Huang and collaborators (2008) used high-capacity adenoviral (HC-Ad) *in vivo* infection, to deliver truncated or full-length HTT-with a poly 128 glutamine repeats of, in the mice striatum. They found differential localization of inclusions: mutant truncated HTT caused very fast formation of inclusions mainly in the nucleus, however, mutant full-length HTT led to a much slower accumulation of inclusions that were localized in the cytoplasm rather than in the nucleus, both *in vitro* and *in vivo*. Interestingly, in HD patients both nuclear and cytoplasmic inclusions have been detected, moreover, neuropil aggregates are prevalent in cortical and striatal neurons (DiFiglia et al., 1997).

Initial studies using adeno-associated virus (AAV) serotype 2 (Senut et al., 2000) or LV vectors (de Almeida et al., 2002) to express mHTT, recapitulate some key elements of the disease and resulted in a limited degree of neurodegeneration 5-8 weeks after injection into the striata of rats. A behavioral phenotype was not characterized in these studies. Also in our model a preliminary behavioral experiments aimed to evaluate the loco-motor coordination was conducted and our animals behaved normally. This occurrence is most probably due to mono-lateral degeneration induced by our experimental protocol. A non-human primate model of HD, generated by LV injection to the macaque putamen, exhibiting striatal neurodegeneration and a progressive motor phenotype, was described (Palfi et al., 2007). DiFiglia and collaborators, also reported a robust and rapid onset phenotype characterized by striatal neurodegeneration and behavioral impairment in mice as early as 2 weeks after AAV injection (DiFiglia et al., 2007).

Many studies have consistently shown that the degenerative process does not equally affect all striatal neurons, but preferentially affects GABAergic medium-sized spiny neurons (Cicchetti and Parent, 1996, Ferrante et al., 1987, Ruiz and Deglon 2012). The down-regulation of DARPP-32, a mediator of dopamine receptor signaling expressed in 96% of striatal medium-sized spiny neurons, is commonly used as an early marker of neuronal dysfunction induced by mHTT in LV-based HD rat model as well as HD transgenic mice (Luthi-Carter et al., 2000, de Almeida et al., 2002, Bibb et al., 2000).

In human HD brain, there is a relative sparing of striatal interneuron populations that are immune-positive for ChAT (Ferrante et al., 1987). In our model, we observed a significant reduction of all neuronal population analyzed (NeuN, DARPP-32 and ChAT) reflecting the high neuronal tropism of our viral vector. These results are in agreement with those reported for another AAV-based

model, where the over-expression of (construct) induced an almost complete loss of NPY, PARV and ChAT immunoreactivity within the AAV-HD70 striatal expression area in HD model (Franich et al., 2008). In a LV model analysis conducted 12 weeks after injection revealed a substantial survival of NADPH-d interneurons, although in presence of aggregates (de Almeida et al., 2002).

Our model revealed a marked neuroinflammatory response, as activation of glia cells, both astrocytes and microglia. A pronounced astrocytosis accompanied the neuronal loss in the striatum is a well described process (Vonsattel et al., 1985) and more recently a significant role of microglia in HD patients is come out (Politis et al., 2011).

Microglia is the major glial component of the CNS playing a critical role as resident immunocompetent and phagocytic cells, and activated microglia serves as scavenger cell in pathological lesions in the event of infection, inflammation, trauma, ischemia and neurodegeneration in the CNS (Tsuji et al., 2005).

Initial studies showed that microglia activation in HD patients correlates with disease progression as assessed by loss of dopamine D2 receptor binding sites (Pavese et al., 2006; Tai et al, 2007). Interestingly, Tai et al, (Tai et al., 2007b) showed that microglia activation is also evident in presymptomatic HD gene carriers and can be detected up to 15 years before predicted age of onset; moreover a higher level of microglia activation correlates with lower level of dopamine D2 receptor binding sites and was associated with a higher probability of developing HD in 5 years. These findings indicate the microglia activation as an early event associated with subclinical progression of HD (Moller et al., 2010). In our model, microglia appeared to be strongly activated by Q138 injection, determining the appearance of bushy cells, surrounding some mHTT aggregates. If this microglia response is the effort to degrade mHTT aggregates to protect neurons from mHTT toxicity is a matter of debate and needs to be further investigated.

The use of the in vivo localized 1H Magnetic Resonance Spectroscopy (1H-MRS) allows the measure of cerebral metabolites in our model. To our knowledge, these data represent the first evidence of the use of this technique to detected brain metabolite changes in vivo in a viral-injected rodent model and the analogies with the results obtained in patients affected by HD (Sturrock et al. 2010) further demonstrated the validity of our experimental model.

Transcriptional dysregulation is a hallmark of HD and has been assessed in patient's autoptic tissues as well as in several transgenic models such as R6/2 mice. In particular, they are characterized by dysregulation of genes encoding neuronal receptors such as adenosine A2a receptor (ADORA2A, Kuhn et al., 2007; Tarditi et al., 2006), dopamine receptors D1 and D2 (DRD1 and DRD2, Luthi-Carter et al., 2000; Kuhn et al., 2007), cholesterogenic genes like 7DHCR and hmgcoAr (Leoni et al., 2011; Valenza et al., 2007, 2010, Zuccato et al., 2001) and neuropeptides like pro enkefalin

(pENK) (Kuhn et al., 2007). Our quantitative gene expression data demonstrate that our AAV-Q138 rat model recapitulates the transcriptional alteration of genes previously identified in other HD models and in HD patients. These alterations reflect an HD phenotype linked to cholesterol biosynthesis dysfunction and receptor dysregulation.

The positive effect of Cystamine administration on striatal neurodegeneration in our HD rat model, comparable to that achieved by genetic therapy (Franich et al., 2008, Taylor et al., 2013) supports the usefulness of the model as a higher throughput, lower turnover time, bridging in vivo model filling the gap from purely *in vitro/ex vivo* models (primary neuronal cultures, organotypic cultures) to genetic in vivo models for HD.

In conclusion, our comprehensive characterizations demonstrate that our model recapitulates the multiple neuropathological hallmarks of the HD disease (neurodegeneration, protein aggregation, neuroinflammatory events, transcriptional dysregulation and brain metabolite changes), and the possibility to modulate these events may be useful for better understanding the mechanisms at the basis of the pathology.

Acknowledgments

The authors thank Michele Guerrini for excellent technical assistance during the in vivo experiments.

References

Anderson KD, Reiner A. Immunohistochemical localization of DARPP-32 in striatal projection neurons and striatal interneurons: implications for the localization of D1-like dopamine receptors on different types of striatal neurons. Brain Res. 1991; 568: 235-43.

Arlotta P, Molyneaux BJ, Jabaudon D, Yoshida Y, Macklis JD. Ctip2 controls the differentiation of medium spiny neurons and the establishment of the cellular architecture of the striatum. J Neurosci. 2008; 28: 622-32.

Aschauer DF, Kreuz S, Rumpel S. Analysis of transduction efficiency, tropism and axonal transport of AAV serotypes 1, 2, 5, 6, 8 and 9 in the mouse brain. PLoS One. 2013;8: e76310.

Bates GP, Dorsey R, Gusella JF, Hayden MR, Kay C, Leavitt BR, Nance M, Ross CA, Scahill RI, Wetzel R, Wild EJ and Tabrizi S. Huntington disease. Nature Reviews Disease Primers. Article number: 15005 (2015)

Baydyuk M, Xu B. BDNF signaling and survival of striatal neurons. Front Cell Neurosci. 2014; 8: 254.

Bibb JA, Yan Z, Svenningsson P, Snyder GL, Pieribone VA, Horiuchi A, Nairn AC, Messer A, Greengard P. Severe deficiencies in dopamine signaling in presymptomatic Huntington's disease mice. Proc Natl Acad Sci U S A. 2000; 97: 6809-14.

Burger C, Gorbatyuk OS, Velardo MJ, Peden CS, Williams P, Zolotukhin S, Reier PJ, Mandel RJ, Muzyczka N Recombinant AAV viral vectors pseudotyped with viral capsids from serotypes 1, 2, and 5 display differential efficiency and cell tropism after delivery to different regions of the central nervous system. Mol Ther 2004; 10:302-317.

Cicchetti F, Parent A. Striatal interneurons in Huntington's disease: selective increase in the density of calretinin-immunoreactive medium-sized neurons. Mov Disord. 1996; 11: 619-26.

Crotti A, Glass CK. The choreography of neuroinflammation in Huntington's disease. Trends Immunol. 2015; 36: 364-73.

de Almeida LP, Ross CA, Zala D, Aebischer P, Déglon N. Lentiviral-mediated delivery of mutant huntingtin in the striatum of rats induces a selective neuropathology modulated by polyglutamine repeat size, huntingtin expression levels, and protein length. J Neurosci. 2002; 22: 3473-83.

de Backer MW, Fitzsimons CP, Brans MA, Luijendijk MC, Garner KM, Vreugdenhil E, Adan RA An adeno-associated viral vector transduces the rat hypothalamus and amygdala more efficient than a lentiviral vector. BMC Neurosci. 2010; 11:81.

Dedeoglu A, Kubilus JK, Jeitner TM, Matson SA, Bogdanov M, Kowall NW, Matson WR, Cooper AJ, Ratan RR, Beal MF, Hersch SM, Ferrante RJ. Therapeutic effects of cystamine in a murine model of Huntington's disease. J Neurosci. 2002; 22:8942-50.

DiFiglia M, Sapp E, Chase KO, Davies SW, Bates GP, Vonsattel JP, Aronin N. Aggregation of huntingtin in neuronal intranuclear inclusions and dystrophic neurites in brain. Science. 1997; 277:1990-1993.

DiFiglia M, Sena-Esteves M, Chase K, Sapp E, Pfister E, Sass M, Yoder J, Reeves P, Pandey RK, Rajeev KG, Manoharan M, Sah DW, Zamore PD, Aronin N. Therapeutic silencing of mutant huntingtin with siRNA attenuates striatal and cortical neuropathology and behavioral deficits. Proc Natl Acad Sci U S A. 2007; 104: 17204-9.

Fecke W, Gianfriddo M, Gaviraghi G, Terstappen GC, Heitz F. Small molecule drug discovery for Huntington's Disease. Drug Discov Today. 2009; 14: 453-64.

Ferrante RJ. Mouse models of Huntington's disease and methodological considerations for therapeutic trials. Biochim Biophys Acta. 2009, 1792: 506-20.

Ferrante RJ, Beal MF, Kowall NW, Richardson EP Jr, Martin JB. Sparing of acetylcholinesterase-containing striatal neurons in Huntington's disease. Brain Res. 1987; 411:162-6.

Franich NR, Fitzsimons HL, Fong DM, Klugmann M, During MJ, Young D. AAV vector-mediated RNAi of mutant huntingtin expression is neuroprotective in a novel genetic rat model of Huntington's disease. Mol Ther. 2008; 16: 947-56.

Gray M, Shirasaki DI, Cepeda C, Andre VM, Wilburn B, Lu X-H, Tao J, Yamazaki I, Li S-H, Sun Y E, et al. Full-length human mutant huntingtin with a stable polyglutamine repeat can elicit progressive and selective neuropathogenesis in BACHD mice. J Neurosci. 2008; 28:6182–9.5

Grieger JC, Samulski RJ. Adeno-associated virus vectorology, manufacturing, and clinical applications. Methods Enzymol. 2012; 507:229-54.

Ha AD, Fung VS. Huntington's disease. Current Opinion in Neurology 2012; 25: p 491-498.

Huang B, Schiefer J, Sass C, Kosinski CM, Kochanek S.Inducing huntingtin inclusion formation in primary neuronal cell culture and in vivo by high-capacity adenoviral vectors expressing truncated and full-length huntingtin with polyglutamine expansion. J Gene Med. 2008; 10: 269-79.

Huda F, Konno A, Matsuzaki Y, Goenawan H, Miyake K, Shimada T, Hirai H, Distinct transduction profiles in the CNS via three injection routes of AAV9 and the application to generation of a neurodegenerative mouse model. Molecular Therapy - Methods & Clinical Development 2014; 1, 14032.

Ito D, Imai Y, Ohsawa K, Nakajima K, Fukuuchi Y, and Kohsaka S. Microglia-specific localisation of a novel calcium binding protein, Iba1. Brain Res. Mol. Brain Res. 1998; 57:1-9.

Kuhn A, Goldstein DR, Hodges A, Strand AD, Sengstag T, Kooperberg C, Becanovic K, Pouladi MA, Sathasivam K, Cha JH, Hannan AJ, Hayden MR, Leavitt BR, Dunnett SB, Ferrante RJ, Albin R, Shelbourne P, Delorenzi M, Augood SJ, Faull RL, Olson JM, Bates GP, Jones L, Luthi-Carter R. Mutant huntingtin's effects on striatal gene expression in mice recapitulate changes observed in human Huntington's disease brain and do not differ with mutant huntingtin length or wild-type huntingtin dosage. Hum Mol Genet. 2007; 16:1845-61.

La Rosa S, Benicchi T, Bettinetti L, Ceccarelli I, Diodato E, Federico C, Fiengo P, Franceschini D, Gokce O, Heitz F, Lazzeroni G, Luthi-Carter R, Magnoni L, Miragliotta V, Scali C and Valacchi M. Fused 3-Hydroxy-3-trifluoromethylpyrazoles Inhibit Mutant Huntingtin Toxicity ACS Medicinal Chemistry Letters, 2013;4:979-84.

Lee CY, Cantle JP, Yang XW. Genetic manipulations of mutant huntingtin in mice: new insights into Huntington's disease pathogenesis. FEBS J. 2013; 280:4382-94.

Leoni V, Mariotti C, Nanetti L, Salvatore E, Squitieri F, Bentivoglio AR, Bandettini di Poggio M, Piacentini S, Monza D, Valenza M, Cattaneo E, Di Donato S. Whole body cholesterol metabolism is impaired in Huntington's disease. Neurosci Lett. 2011; 494:245-9.

Li SH, Cheng AL, Li H, Li XJ. Cellular defects and altered gene expression in PC12 cells stably expressing mutant huntingtin. J Neurosci 1999; 19:5159-5172.

Li SH, Lam S, Cheng AL, Li XJ. Intranuclear huntingtin increases the expression of caspase-1 and induces apoptosis. Hum Mol Genet. 2000; 9:2859-67.

Luthi-Carter R, Strand A, Peters NL, Solano SM, Hollingsworth ZR, Menon AS, Frey AS, Spektor BS, Penney EB, Schilling G, Ross CA, Borchelt DR, Tapscott SJ, Young AB, Cha JH, Olson JM. Decreased expression of striatal signaling genes in a mouse model of Huntington's disease. Hum Mol Genet. 2000; 9:1259-71.

Mangiarini L, Sathasivam K, Seller M, Cozens B, Harper A, Hetherington C, Lawton M, Trottier Y, Lehrach H, Davies SW, Bates GP. Exon 1 of the HD gene with an expanded CAG repeat is sufficient to cause a progressive neurological phenotype in transgenic mice. Cell. 1996; 87:493-506.

McFarland NR, Lee JS, Hyman BT, McLean PJ Comparison of transduction efficiency of recombinant AAV serotypes 1, 2, 5, and 8 in the rat nigrostriatal system. J Neurochem 2009; 109:838-845.

Menalled LB Knock-in mouse models of Huntington's disease. NeuroRx. 2005; 2: 465-70.

Menalled L, Brunner D. Animal models of Huntington's disease for translation to the clinic: best practices. Mov Disord. 2014; 29:1375-90.

Möller T. Neuroinflammation in Huntington's disease. J Neural Transm. 2010; 117:1001-8.

Myers RH, Vonsattel JP, Stevens TJ, Cupples LA, Richardson EP, Martin JB, Bird ED. Clinical and neuropathologic assessment of severity in Huntington's disease. Neurology. 1988; 38:341-7.

Ouimet CC, Langley-Gullion KC, Greengard P. Quantitative immunocytochemistry of DARPP-32-expressing neurons in the rat caudatoputamen. Brain Res. 1998; 808: 8-12.

Otsu, N., "A Threshold Selection Method from Gray-Level Histograms," IEEE Transactions on Systems, Man, and Cybernetics, Vol. 9, No. 1, 1979, pp. 62-66.

Palfi S, Brouillet E, Jarraya B, Bloch J, Jan C, Shin M, Condé F, Li XJ, Aebischer P, Hantraye P, Déglon N. Expression of mutated huntingtin fragment in the putamen is sufficient to produce abnormal movement in non-human primates. Mol Ther. 2007; 15:1444-51.

Pavese N, Gerhard A, Tai YF, Ho AK, Turkheimer F, Barker RA, Brooks DJ, Piccini P. Microglial activation correlates with severity in Huntington disease: a clinical and PET study. Neurology. 2006; 66:1638-43.

Paxinos G. and Watson C. (1998) The Rat Brain in Stereotaxic Coordinates Fourth Edition. Academic Press, San Diego.

Politis M, Pavese N, Tai YF, Kiferle L, Mason SL, Brooks DJ, Tabrizi SJ, Barker RA, Piccini P. Microglial activation in regions related to cognitive function predicts disease onset in Huntington's disease: a multimodal imaging study. Hum Brain Mapp. 2011; 32: 258-70.

Politis M, Lahiri N, Niccolini F, Su P, Wu K, Giannetti P, Scahill RI, Turkheimer FE, Tabrizi SJ, Piccini P. Increased central microglial activation associated with peripheral cytokine levels in premanifest Huntington's disease gene carriers. Neurobiol Dis. 2015; 83: 115-121.

Popiel HA, Takeuchi T, Fujita H, Yamamoto K, Ito C, Yamane H, Muramatsu S, Toda T, Wada K, Nagai Y. Hsp40 gene therapy exerts therapeutic effects on polyglutamine disease mice via a non-cell autonomous mechanism. PLoS One. 2012;7: e51069.

Ramaswamy S, McBride JL, Kordower JH Animal models of Huntington's disease. ILAR J 2007; 48:356-373.

Régulier E, Trottier Y, Perrin V, Aebischer P, Déglon N. Early and reversible neuropathology induced by tetracycline-regulated lentiviral overexpression of mutant huntingtin in rat striatum. Hum Mol Genet. 2003; 12: 2827-36. Epub 2003 Sep 2.

Ross CA, Tabrizi SJ. Huntington's disease: from molecular pathogenesis to clinical treatment. Lancet Neurol. 2011; 10:83-98.

Ruiz M, Déglon N. Viral-mediated overexpression of mutant huntingtin to model HD in various species. Neurobiol Dis. 2012; 48: 202-11. Epub 2011 Aug 25

Schilling G, Becher MW, Sharp AH, Jinnah HA, Duan K, Kotzuk JA, Slunt HH, Ratovitski T, Cooper JK, Jenkins NA, Copeland NG, Price DL, Ross CA, Borchelt DR. Intranuclear inclusions and neuritic aggregates in transgenic mice expressing a mutant N-terminal fragment of huntingtin. Hum Mol Genet. 1999; 8: 397-407.

Senut MC, Suhr ST, Kaspar B, Gage FH Intraneuronal aggregate formation and cell death after viral expression of expanded polyglutamine tracts in the adult rat brain. J Neurosci 20:219-229.2000.

Slow EJ, van Raamsdonk J, Rogers D, Coleman SH, Graham RK, Deng Y, Oh R, Bissada N, Hossain SM, Yang Y Z, et al. Selective striatal neuronal loss in a YAC128 mouse model of Huntington disease. Hum Mol Genet. 2003; 12:1555–67.

Smith MR, Syed A, Lukacsovich T, Purcell J, Barbaro BA, Worthge SA, Wei SR, Pollio G, Magnoni L, Scali C, Massai L, Franceschini D, Camarri M, Gianfriddo M, Diodato E, Thomas R, Gokce O, Tabrizi SJ, Caricasole A, Landwehrmeyer B, Menalled L, Murphy C, Ramboz S, Luthi-Carter R, Westerberg G, Marsh JL. A potent and selective Sirtuin 1 inhibitor alleviates pathology in multiple animal and cell models of Huntington's disease. Hum Mol Genet. 2014; 23: 2995-3007.

Sturrock A, Laule C, Decolongon J, Dar Santos R, Coleman AJ, Creighton S, Bechtel N, Reilmann R, Hayden MR, Tabrizi SJ, Mackay AL, Leavitt BR. Magnetic resonance spectroscopy biomarkers in premanifest and early Huntington disease. Neurology. 2010 9; 75:1702-10.

Tai YF, Pavese N, Gerhard A, Tabrizi SJ, Barker RA, Brooks DJ, Piccini P. Imaging microglial activation in Huntington's disease. Brain Res Bull. 2007; 72:148-51. Epub 2006 Nov 27.

Tai YF, Pavese N, Gerhard A, Tabrizi SJ, Barker RA, Brooks DJ, Piccini P. Microglial activation in presymptomatic Huntington's disease gene carriers. Brain. 2007; 130:1759-66. Epub 2007 Mar 30.

Tarditi A, Camurri A, Varani K, Borea PA, Woodman B, Bates G, Cattaneo E, Abbracchio MP. Early and transient alteration of adenosine A2A receptor signaling in a mouse model of Huntington disease. Neurobiol Dis. 2006; 23:44-53. Epub 2006 May 2.

Taylor DM, Moser R, Régulier E, Breuillaud L, Dixon M, Beesen AA, Elliston L, Silva Santos Mde F, Kim J, Jones L, Goldstein DR, Ferrante RJ, Luthi-Carter R. MAP kinase phosphatase 1 (MKP-1/DUSP1) is neuroprotective in Huntington's disease via additive effects of JNK and p38 inhibition. J Neurosci. 2013; 33:2313-25.

Tenenbaum L, Chtarto A, Lehtonen E, Velu T, Brotchi J, Levivier M (Recombinant AAV-mediated gene delivery to the central nervous system. J Gene Med 6 Suppl 1: S212-S222.2004).

The Huntington's Disease Collaborative Research Group. A novel gene containing a trinucleotide repeat that is expanded and unstable on Huntington's disease chromosomes. Cell 1993; 72:971-983.

Tsuji D, Kuroki A, Ishibashi Y, Itakura T, Kuwahara J, Yamanaka S, Itoh K. Specific induction of macrophage inflammatory protein 1-alpha in glial cells of Sandhoff disease model mice associated with accumulation of N-acetylhexosaminyl glycoconjugates. J Neurochem. 2005; 92:1497-507.

Valenza M, Cattaneo E. Emerging roles for cholesterol in Huntington's disease. Trends Neurosci. 2011; 34: 474-86.

Valenza M, Leoni V, Tarditi A, Mariotti C, Björkhem I, Di Donato S, Cattaneo E. Progressive dysfunction of the cholesterol biosynthesis pathway in the R6/2 mouse model of Huntington's disease. Neurobiol Dis. 2007; 28:133-42. Epub 2007 Jul 10.

Valenza M, Leoni V, Karasinska JM, Petricca L, Fan J, Carroll J, Pouladi MA, Fossale E, Nguyen HP, Riess O, MacDonald M, Wellington C, DiDonato S, Hayden M, Cattaneo E. Cholesterol defect is marked across multiple rodent models of Huntington's disease and is manifest in astrocytes. J Neurosci. 2010; 30:10844-50.

Van Raamsdonk JM, Pearson J, Bailey CD, Rogers DA, Johnson GV, Hayden MR, Leavitt BR. Cystamine treatment is neuroprotective in the YAC128 mouse model of Huntington disease. J Neurochem. 2005; 95: 210-20.

Wilson M1, Reynolds G, Kauppinen RA, Arvanitis TN, Peet AC. A constrained least-squares approach to the automated quantitation of in vivo ^{1}H magnetic resonance spectroscopy data. Magn Reson Med. 2011; 65:1-12.

Vonsattel JP, Myers RH, Stevens TJ, Ferrante RJ, Bird ED, Richardson EP Jr. Neuropathological classification of Huntington's disease. J Neuropathol Exp Neurol. 1985; 44: 559-77.

Wyttenbach A, Swartz J, Kita H., Thykjaer T, Carmichael J, Bradley J, Brown R, Maxwell M, Schapira A, Orntoft TF, et al. Polyglutamine expansions cause decreased CRE-mediated transcription and early gene expression changes prior to cell death in an inducible cell model of Huntington's disease. Hum. Mol. Genet. 2001; 10: 1829–1845.

Zala D, Benchoua A, Brouillet E, Perrin V, Gaillard MC, Zurn AD, Aebischer P, Déglon N. Progressive and selective striatal degeneration in primary neuronal cultures using lentiviral vector coding for a mutant huntingtin fragment. Neurobiol Dis. 2005; 20: 785-98. Epub 2005 Jul 11.

Zhu X, Schuff N, Kornak J, Soher B, Yaffe K, Kramer JH, Ezekiel F, Miller BL, Jagust WJ, Weiner MW. Effects of Alzheimer disease on fronto-parietal brain N-acetyl aspartate and myo-inositol using magnetic resonance spectroscopic imaging. Alzheimer Dis Assoc Disord. 2006; 20: 77-85.

Zuccato C, Ciammola A, Rigamonti D, Leavitt BR, Goffredo D, Conti L, MacDonald ME, Friedlander RM, Silani V, Hayden MR, Timmusk T, Sipione S, Cattaneo E. Loss of huntingtin-mediated BDNF gene transcription in Huntington's disease. Science. 2001; 20; 293: 493-498. Epub 2001 Jun 14.

Figure Legends

Fig. 1 Panel A: Schematic representation of the site of injection of the two viral preparations in rat brain. Four microliters ($15.2x10^{10}$GC) of AAV-Exon1-Q138-GFP and AAV-Exon1-Q17-GFP were injected in the right and in the left striatum respectively, (0.5 mm anterior; ±3.0 mm lateral to Bregma and 4.8 mm depth from dura) by a Hamilton syringe equipped with a 30 gauge blunt-tip. Panel B: microphotograph showing the GFP epiflourescence in the injected striata. Panel C-D: Confocal microphotograph of AAV9-Ex1-AcGFP-Q17 (C) and AAV9-Ex1-AcGFP-Q138 (D) illustrating the GFP signal. Note the diffused GFP signal in the entire striatal area of Q17- injected striatum while the injection of mHTT determined massive production of GFP positive aggregates in the entire striatal area; scale bar: 100 µm. Panel E: microphotograph showing the EM-48 immunolabeling (black aggregates) in the AAV-Exon1-Q138-injected striatum Scale bar: 50 µm. Panels F-H Confocal microphotographs of the AAV-Exon1-Q17-injected striatum (F) and the AAV-Exon1-Q138-injected striatum (G) illustrating the immunoreactivity for NeuN (red) and GFAP (sky blue) and GFP epifluorescence (green), merge: note that GFP-mHTT aggregates are mostly expressed in neurons; Panel H, activated microglia exerts macrophagic functions on mHTT aggregates. Confocal microphotographs of mHTT aggregates (DAPI epifluorescence, blue, GFP epifluorescence, green, and Iba-1, red) immunoreactivity in the AAV-Exon1-Q138-GFP-injected striatum. Scale bar: 20 µm.

Fig. 2 Neurodegenerative damage induced by mHTT aggregates expression- Panels A-I: Bright Field microphotographs of the NeuN (A-C), DARPP-32 (D-F) and ChAT (G-I) immunoreactivity in coronal slides (panels A, D and G, 1X) and in AAV-Exon1-Q17-injected (panels B, E and H) and the AAV-Exon1-Q138-GFP-injected (panels C, F and I) striatum. Scale bar: B-C, E-F,: 100 µm. Scale bar: H-I: 50 µm Panels L-N: histograms of NeuN, DARPP-32 and ChAT immunoreactivity quantification (number of cells or Positive Pixel Counts per area) in the Q17 (white) and Q138 (grey) injected striatum. Paired T-test analysis revealed that mHTT injection significantly decreased the amount of NeuN, DARPP-32 and ChAT immunoreactivity in respect to WT HTT injection. *$P<0.05$ and ** $P< 0.001$.

Fig. 3 Neuroinflammatory reaction induced by mHTT aggregates expression. Panels A-F: Bright Field microphotographs of the Iba-1 (Panels A-C) and GFAP (Panels D-F) immunoreactivity in coronal slides (Panels A and D, 1X) and in AAV-Exon1-Q17-injected (Panels B and E) and the AAV-Exon1-Q138-GFP-injected (Panels C and F) striatum. Note the strong inflammatory reaction in the right striatum in comparison to contralateral. Scale bar: 50 µm. Panels G-: histograms of Iba-1 and GFAP quantification in the Q17 (white) and Q138 (grey) injected striatum. Paired T-test

analysis revealed that mHTT injection significantly increased the amount of Iba-1 and GFAP positive cells in respect to WT HTT injection. * P< 0.05 and ** P< 0.001.

Fig. 4 mHTT induced selective gene expression modulation. Quantitative RT-PCR detection of the expression of: 7DHCR, pENK, ADORA2A, DRD1 and DRD2 in the striata obtained from animals injected with WT HTT (Q17) and m-HTT (Q138) in the left and in the right striatum, respectively. Data are expressed as ratio of Q138/Q17. The Q138 injection significantly decreased the expression of 7DHCR, pENK, ADORA2A, DRD1 and DRD2. * P< 0.05 and ** P< 0.01.

Fig. 5 mHTT induced alteration of striatal metabolism detected by H^1 Magnetic Resonance Spectroscopy (H^1-MRS). Panel A and B: H^1-MRS spectra from voxels in the Q17 and Q138 - injected striatum, respectively. Panel C and D: histograms of Myo-Ins/Cr and tNAA/Cr quantification. Paired t-test analysis showed that m-HTT injection significantly increased Myo-Ins and decreased tNAA concentrations. *P<0.05 for both.

Fig. 6 Effects of Cystamine on NeuN immunoreactivity in the striatum. Panels A-B: Representative Bright Field microphotographs of the NeuN in Q138-injected striatum of Vehicle (A), Cystamine (B) treated animals. Scale bar: 50 µm. Panel C: Histograms of the ratio of NeuN quantification in the Q138 and Q17 injected striatum in animals treated with vehicle (white), Cystamine (light grey) for 21 days. One-way ANOVA analysis revealed that Cystamine significantly increased the ratio of Q138/Q17 NeuN positive cells in respect to vehicle treated animals. * P< 0.01. Panel D: Histograms of the ratio of DARPP-32 quantification in the Q138 and Q17 injected striatum in animals treated with vehicle (white), Cystamine (light grey) for 21 days. One-way ANOVA analysis revealed only a tendency to increase the ratio of Q138/Q17 DARPP-32 positive cells (P= 0.06).

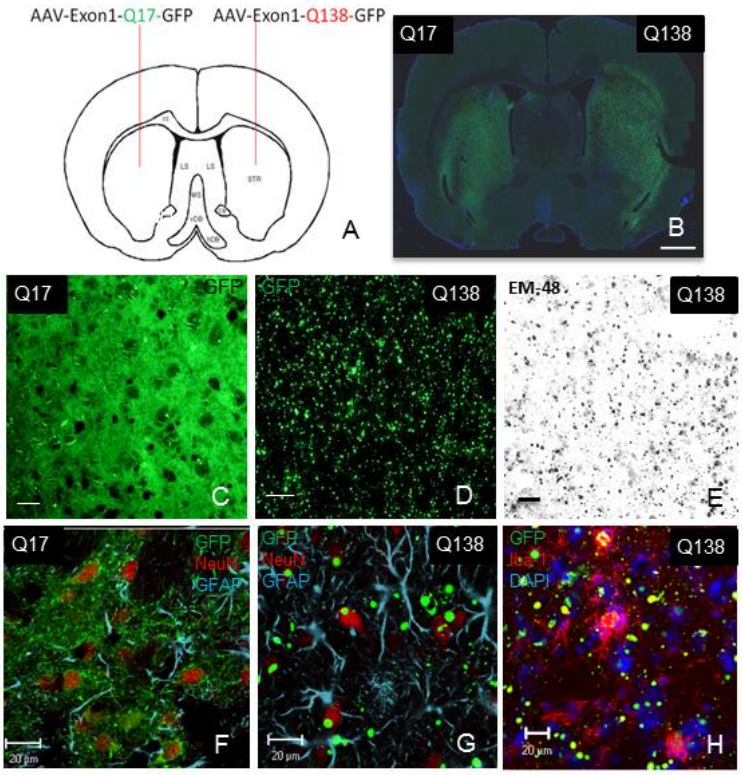

Fig. 1

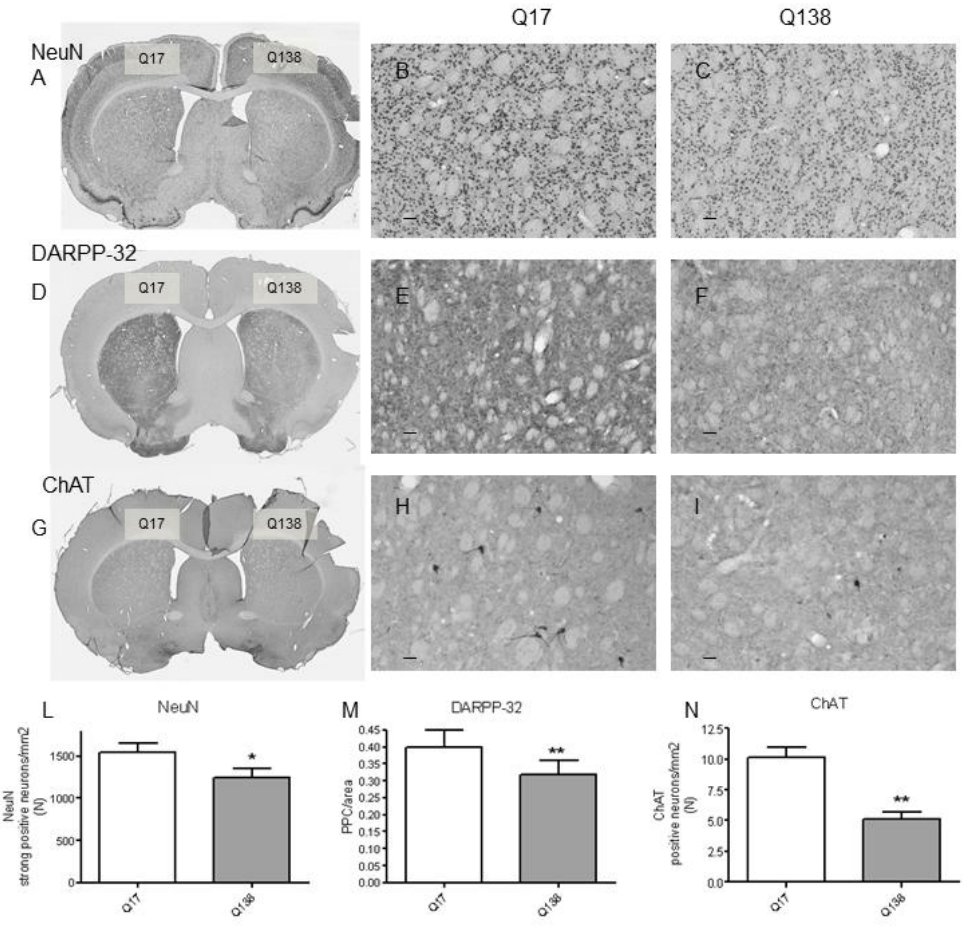

Fig. 2

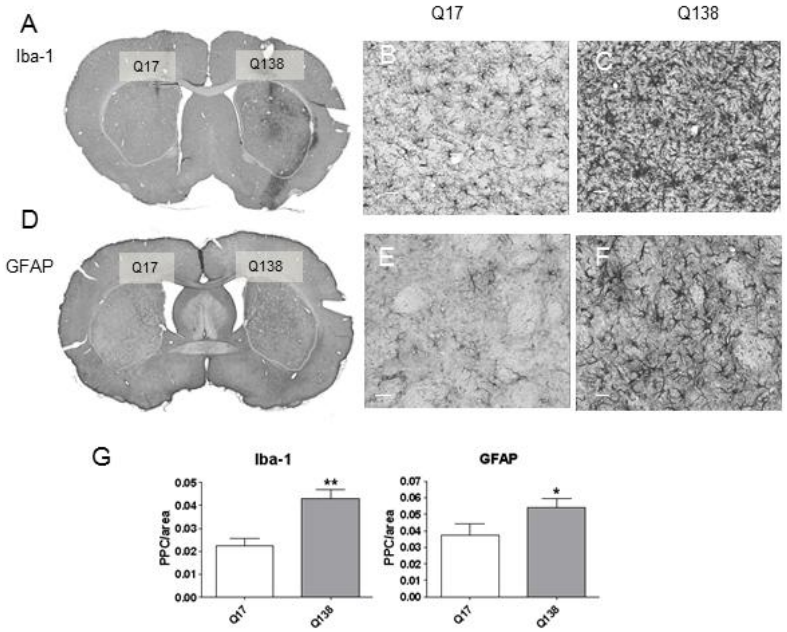

Fig. 3

RnPENKfwd	CAACCGTGCGAAAGATAGCCA
RnPENKrev	CCATACCTCTTGCTCGTGCTG
RnAdora2Afwd	CCATCCCCTTCGCTATCACC
RnAdora2Arev	AAGCCATTGTACCGGAGTGG
RnDRD1Afwd	CTGTCACTGCTCATCCTGTCC
RnDRD1Arev	ACCTTGGACCTCAGGTGTCGA
Rn7DHCRfor	CGTCCAAGAAGGTGCCATAAC
Rn7DHCRrev	AGCGTTCACAAACCAGAGGAAG
RnDrd2fwd	GCCACACTGGTAATGCCGTG
RnDrd2rev	AATGCTGATGGCACACAGGTTCA
RnActinBfwd	ACCCTAAGGCCAACCGTGAA
RnActinBrev	ATGCCAGTGGTACGACCAGA

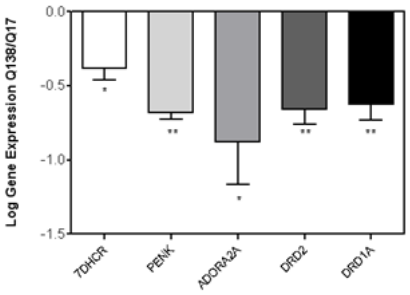

Fig. 4

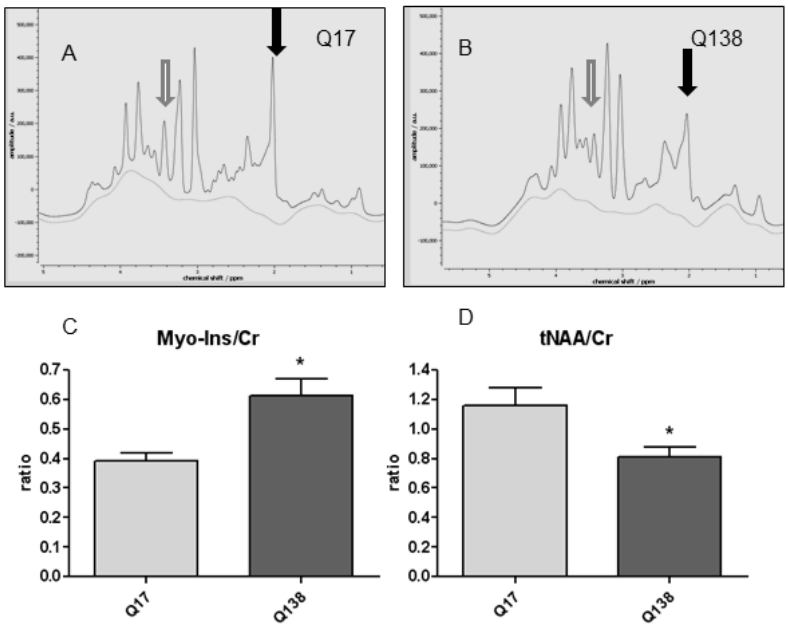

Fig. 5

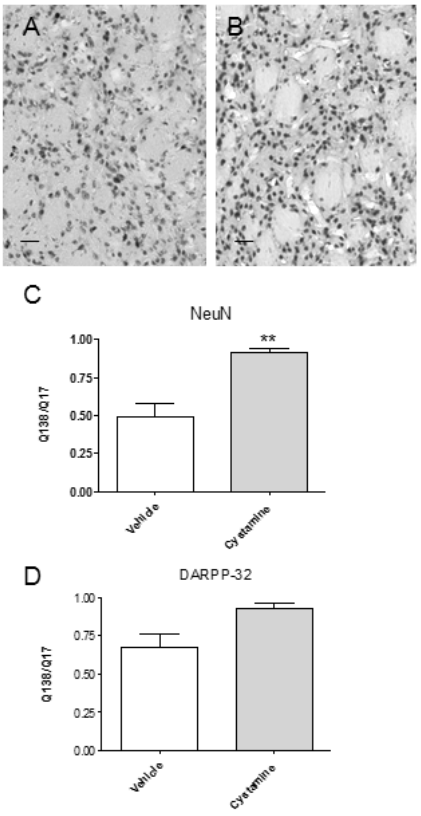

Fig. 6

Highlights

- rAAV2/9-Exon 1 HTT 17 or 138 CAG was used to create a new rat model of HD.
- Exon 1 HTT-Q138 induced neurodegeneration and neuroinflammation in the striatum.
- Genomic analysis and H^1-MRS study revealed high association with human HD hallmarks.
- We pharmacologically validated our model using cystamine.
- Our model provide useful tool for drug discovery process.